



ELSEVIER

## Performance of the CAPRICE RICH detector during the 1994 balloon flight

G. Barbiellini<sup>j</sup>, G. Basini<sup>g</sup>, R. Bellotti<sup>k</sup>, M. Bocciolini<sup>h</sup>, M. Boezio<sup>j</sup>, F. Massimo Brancaccio<sup>h</sup>, U. Bravar<sup>j</sup>, F. Cafagna<sup>k</sup>, M. Candusso<sup>i</sup>, P. Carlson<sup>d</sup>, M. Casolino<sup>i</sup>, M. Castellano<sup>k</sup>, G. De Cataldo<sup>k</sup>, M. Circella<sup>k</sup>, A. Codino<sup>f</sup>, N. Finetti<sup>f</sup>, T. Francke<sup>d,\*</sup>, N. Giglietto<sup>k</sup>, R.L. Golden<sup>a</sup>, C. Grimani<sup>f</sup>, M. Hof<sup>l</sup>, B. Marangelli<sup>k</sup>, C.N. De Marzo<sup>k</sup>, J.W. Mitchell<sup>c</sup>, A. Morselli<sup>i</sup>, M.P. De Pascale<sup>i</sup>, P. Papini<sup>h</sup>, A. Perego<sup>h</sup>, S. Piccardi<sup>h</sup>, P. Picozza<sup>i</sup>, M. Ricci<sup>g</sup>, P. Schiavon<sup>j</sup>, M. Simon<sup>i</sup>, R. Sparvoli<sup>i</sup>, P. Spillantini<sup>h</sup>, P. Spinelli<sup>k</sup>, S.A. Stephens<sup>b</sup>, S.J. Stochaj<sup>a</sup>, R.E. Streitmatter<sup>c</sup>, M. Suffert<sup>e</sup>, A. Vacchi<sup>j</sup>, N. Weber<sup>d</sup>, N. Zampa<sup>j</sup>

<sup>a</sup>Particle Astrophysics Lab, New Mexico State Univ., Las Cruces, NM, USA

<sup>b</sup>Tata Institute of fundamental Research, Bombay, India

<sup>c</sup>Goddard Space Flight center/NASA, Greenbelt, MD, USA

<sup>d</sup>Royal Institute of Technology, Stockholm, Sweden

<sup>e</sup>Centre de Recherches Nucléaires, Strasbourg, France

<sup>f</sup>Dipartimento di Fisica dell'Univ. di Perugia and INFN-Sezione di Perugia, Perugia, Italy

<sup>g</sup>INFN Laboratori Nazionali di Frascati, Frascati, Italy

<sup>h</sup>Dipartimento di Fisica dell'Univ. di Firenze and INFN-Sezione di Firenze, Florence, Italy

<sup>i</sup>Dipartimento di Fisica dell'Univ. di Roma II "Tor Vergata" and INFN-Sezione di Roma II "Tor Vergata", Roma, Italy

<sup>j</sup>Dipartimento di Fisica dell'Univ. di Trieste and INFN-Sezione di Trieste, Trieste, Italy

<sup>k</sup>Dipartimento di Fisica dell'Univ. di Bari and INFN-Sezione di Bari, Trieste, Italy

<sup>l</sup>University of Siegen, Siegen, Germany

### Abstract

A RICH detector capable of detecting unit charged particles, e.g. antiprotons and positrons, has been used successfully for the first time in a balloon-borne magnet spectrometer. The thin and compact CAPRICE RICH detector uses a NaF solid radiator, TMAE vapour as photo converter and cathode pad readout in the photosensitive MWPC operated at low gain. 15 photoelectrons are detected per ring for  $\beta = 1$ , perpendicular incidence particles giving a resolution on the Cherenkov angle of 8 mrad, increasing to 14 mrad at 20° incidence angle. Besides particle identification on an event-by-event basis it efficiently rejects multiparticle events and albedo particles.

### 1. Introduction

The Cosmic AntiParticle Ring Imaging Cherenkov Experiment (CAPRICE) has for the first time used a RICH detector in a balloon-borne magnet spectrometer that is sensitive to unit charged particles. Previously, the Chicago University group [1] has flown a gas-Rich detector sensitive to helium and higher charges.

The aim of the experiment is to measure the flux of antimatter, mainly antiprotons and positrons, and light isotopes in the cosmic radiation. Sophisticated particle identification detectors are needed to identify the rare antiprotons in a large background of electrons, muons and

protons, and the positrons in an even larger background of protons.

The NMSU/WiZard CAPRICE spectrometer [2] is shown in Fig. 1 and includes from top to bottom: a solid radiator RICH detector, scintillators for time-of-flight and  $dE/dx$  measurements, a super conducting magnet with a tracking system of multiwire proportional chambers (MWPC) and drift chambers [3], and an electromagnetic Si-W calorimeter ( $7X_0$ ) [4,5].

The flight took place from Lynn Lake, Manitoba, Canada, on August 8–9, 1994. Data was successfully collected during the 3.5 h long ascent and for 23 h at a float altitude above 36 km (less than 5 g/cm<sup>2</sup> residual atmosphere). Totally, data from more than 6 million cosmic rays were recorded. All detectors worked well during the flight.

\* Corresponding author.

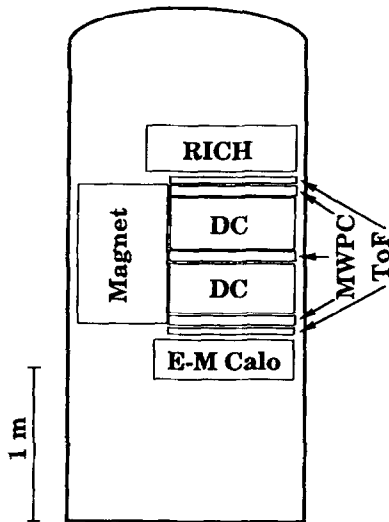


Fig. 1. The CAPRICE magnet spectrometer.

The performance of the RICH detector during the flight is presented below.

## 2. The CAPRICE RICH detector

The CAPRICE RICH detector is shown in Fig. 2. Cherenkov light is emitted in a 10 mm thick solid radiator of NaF when a charged particle transverses the detector if  $\beta > 1/n$  ( $\beta$  is the particle velocity relative to the speed of light,  $n$  is the refractive index of NaF). The cone of light refracts out of the crystal and is expanded in a nitrogen volume before entering into a photosensitive MWPC. The Cherenkov photons are converted into photoelectrons by the photosensitive compound tetrakis-(dimethylamino)-ethylene (TMAE) [6], and are amplified in a MWPC. The induced pulse in the cathode pad plane is detected and gives an unambiguous image of the Cherenkov light. The MWPC is operated at low gain (a few times  $10^4$ ) with pure

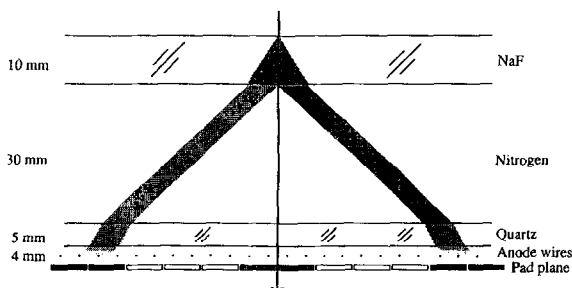


Fig. 2. A schematic view of the CAPRICE RICH detector. A 1.7 GeV/c antiproton event is indicated. The Cherenkov light emitted in the NaF is detected in a photosensitive MWPC with pad readout after expansion in nitrogen.

ethane as amplification gas. The size of the cathode pads is 8 by 8 mm<sup>2</sup>.

The TMAE itself acts as an oxysorb and cleans the amplification gas as it bubbles through the liquid TMAE before entering the detector. During the flight, a continuous flow of ethane was used (3 l/h) and the TMAE was heated to 38°C. The detector was kept at 45°C to avoid condensation of TMAE.

The RICH detector and the results from particle beam tests are described in more detail in Ref. [7].

## 3. Experimental results

### 3.1. Single events

The image of the Cherenkov light is a ring at perpendicular incidence angle which opens up to a wide U-shape at inclined incidence. Fig. 3 shows four single events collected during the flight: a) a 1.5 GeV kinetic energy proton at 1° incidence angle, b) a 1.5 GeV proton at 10° incidence angle, c) a 1.1 GeV/nucleon <sup>4</sup>He at 2° incidence angle and d) a 1.5 GeV/nucleon <sup>4</sup>He at 20° incidence angle towards the detector, which is the maximum incidence angle during the experiment. The image of the Cherenkov light is well separated from the ionization of the chamber gas by the particle (the central spot) for particles with  $\beta > 0.85$  also for large angle of incidence.

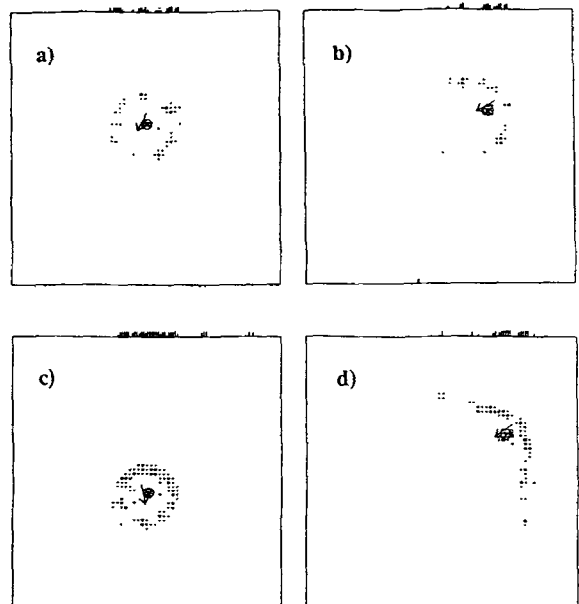


Fig. 3. Single events from the flight. a) a 1.5 GeV proton at 1°, b) a 1.5 GeV proton at 10°, c) a 1.1 GeV/nucleon <sup>4</sup>He at 2°, and d) a 1.5 GeV/nucleon <sup>4</sup>He at 20°. The arrow indicates the direction of the particle.

### 3.2. Multiparticle rejection

The induced pulse from the ionization of the chamber gas by the particle is used to get a redundant measurement of the impact point of the charged particle with the RICH, independent of the tracking system. Fig. 4 shows the distance between the predicted impact point from the tracking system (known with a precision better than  $200\ \mu\text{m}$ ) and a center-of-gravity calculation of the central 25 pads around the pad with the largest signal, for all events with at least one reconstructable track. The resolution of the center of gravity calculation for clean single tracks is  $1.4\ \text{mm}$  independent of incidence angle. This quantity has shown to be a powerful tool for rejecting multiparticle events where two or more charged particles pass through the RICH close to each other, e.g. from interactions in the RICH itself. This will disturb the center-of-gravity calculation and give a value different from the tracking prediction.

The amplitude in the pads is another useful tool for rejecting multiparticle events when the particles are more than  $2\ \text{cm}$  apart. A charged particle gives a pulse height close to saturation in the electronics while a signal originating from a Cherenkov photon is significantly smaller. This property is also useful for detector alignment.

### 3.3. Particle identification

The particle identification properties of the RICH detector are illustrated in Fig. 5. The reconstructed Cherenkov angle versus rigidity (momentum/charge) for unit charged

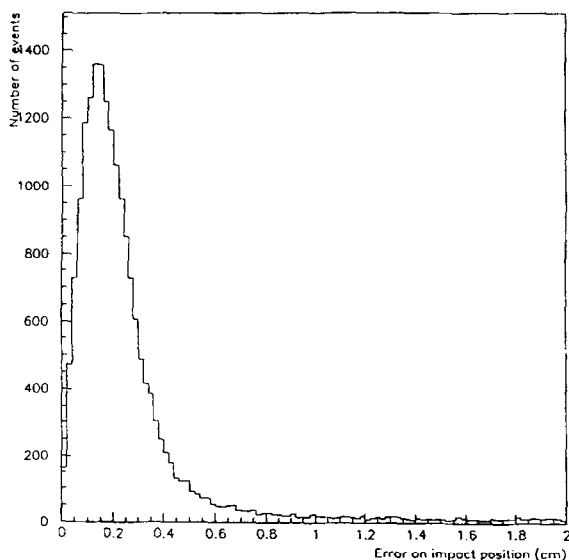


Fig. 4. Resolution of the impact position of the particle with the RICH using RICH along. The tail is due to several charged particles traversing the detector.

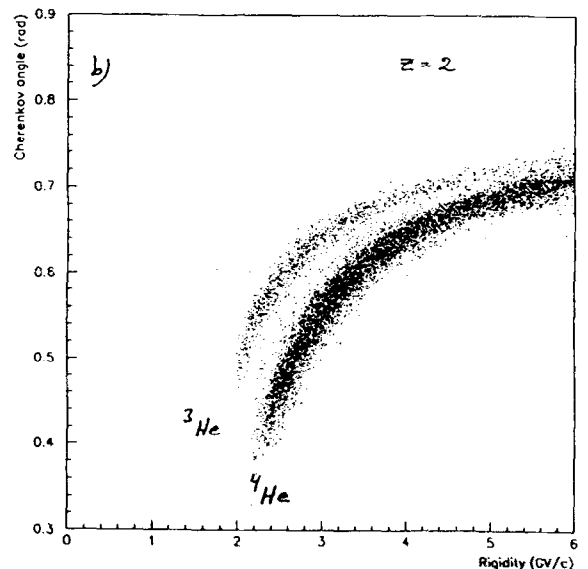
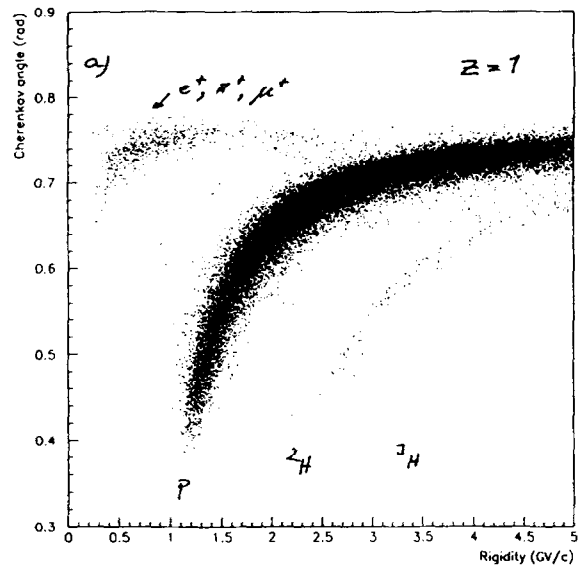


Fig. 5. Reconstructed Cherenkov angle versus rigidity (momentum/charge) for a)  $Z = 1$  and b)  $Z = 2$  particles at float altitude.

particles as selected by  $dE/dx$  in the two scintillators is shown in Fig. 5a and ditto for charge two particles in Fig. 5b. As shown in the figure the RICH is capable of isotope identification ( $^2\text{H}$ ,  $^3\text{H}$ ,  $^3\text{He}$  and  $^4\text{He}$ , etc.) as well as (anti)proton identification in a large background of  $\beta = 1$  particles.

The resolution of the Cherenkov angle during the flight is shown in Fig. 6. The resolution (rms) as functions of incidence angle for particles with  $\beta > 0.95$  is presented in Fig. 6a and the resolution (rms) as a function of  $\beta$  for particles of all incidence angles ( $0^\circ$ – $20^\circ$ ) in Fig. 6b. The threshold for emission of Cherenkov light in NaF is  $\beta =$

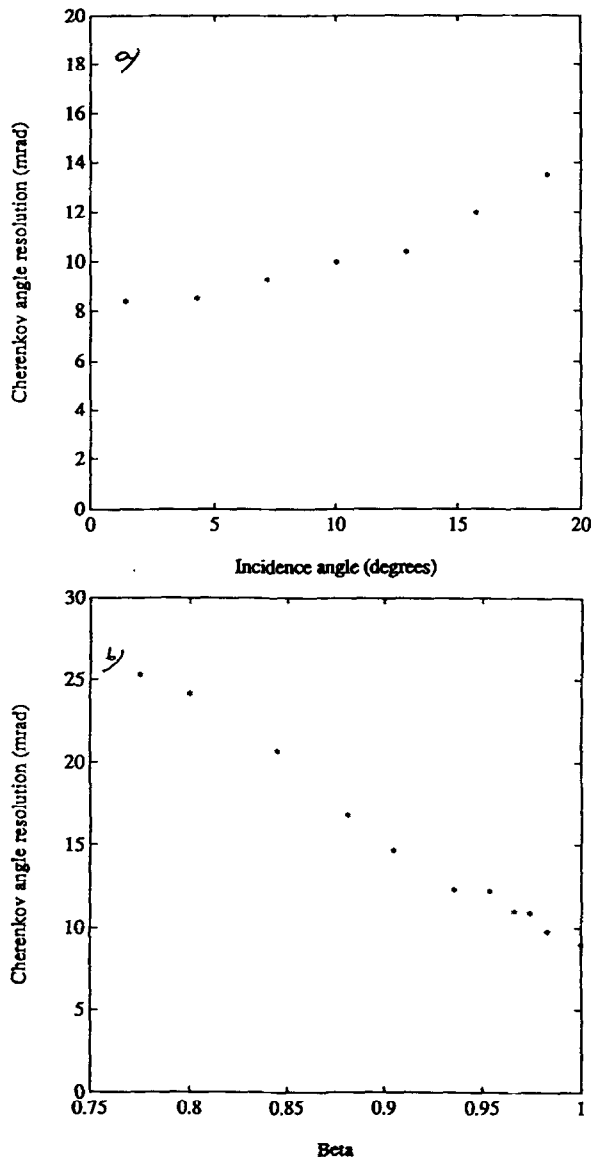


Fig. 6. Resolution on the Cherenkov angle as a function of a) incidence angle of the particle for  $\beta > 0.95$  particles, and b)  $\beta$  for particles of all incidence angles ( $0^\circ$ – $20^\circ$ ).

0.75, but the particles need to have  $\beta > 0.85$  with the geometry used to clearly separate the image of the Cherenkov light from the ionization of the particle. The resolution of the Cherenkov angle during the flight was slightly worse than during the beam tests due to significantly pressure changes (30%) inside the gondola during the flight. The anode voltage was adjusted continuously to compensate for gain variations. The number of photoelectrons detected per event for  $\beta = 1$  particles at perpendicular incidence is around 15 during the flight compared to 21 during the beam tests [7].

### 3.4. Albedo rejection

In space experiments it is important to separate between downward and upward (albedo) moving particles, since an albedo proton can mimic a downward moving antiproton. Traditionally this is done using time-of-flight between two scintillators, where the upper scintillator should give a signal before the lower. The directional sensitivity of a RICH detector has proven to be powerful for albedo discrimination. Out of 3245 albedo particles, with only one charged track through the spectrometer and with a velocity large enough to emit Cherenkov light, none has an image that could mimic a Cherenkov light image even with the loosest cuts. Note that the NaF crystals are polished on all sides, and not painted on the top to absorb Cherenkov light going upwards.

### 3.5. Cherenkov angle reconstruction algorithm

For Cherenkov light imaging it is essential that the refractive index of the radiator is less than  $\sqrt{2}$ , not to trap the Cherenkov light inside the radiator by total reflection. NaF is the only solid material with a refractive index less than  $\sqrt{2}$  in the wavelength region where the CAPRICE RICH is sensitive (170–220 nm) [7–8]. However, the refractive index is close to  $\sqrt{2}$  and part of the Cherenkov light will be trapped inside the NaF crystals by (total) reflections, especially photons of short wavelength and at inclined incidence angles of the particle. This implies that the mean wavelength of the Cherenkov photons that are detected in the photosensitive MWPC depends on the incidence angle and on the  $\beta$  of the incoming particle. Furthermore, for small  $\beta$  and large incidence angles the Cherenkov light image partly overlap with the ionization of the chamber gas by the particle, and only the pads outside the ionization region can be used in the fit of the Cherenkov angle. This bias the Cherenkov angle in such a way that photoelectrons near the ionization will not be included in the fit of the whole image.

This has to be taken into account when reconstructing the Cherenkov angle of an event. One way to compensate for this effect is to use a “compensated” refractive index of NaF in the reconstruction algorithm that is a function of the particle incidence angle  $\theta$  and velocity  $\beta$ . Fig. 7 shows the “compensated” refractive index of NaF as a function of  $\theta$  and  $\beta$  that best fits a clean proton sample. The effect is large for small  $\beta$  and inclined incidence angles. Using such a “compensated” refractive index instead of a constant value significantly increases the Cherenkov angle resolution. A different “compensated” refractive index is used for charge two particles.

## 4. Conclusion

A RICH detector sensitive to unit charged particles has been used for the first time in a balloon-borne magnet

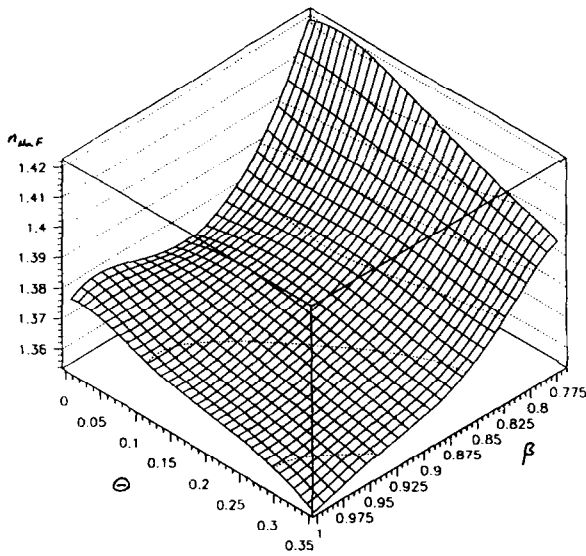


Fig. 7. "Compensated" refractive index of NaF used in the reconstruction algorithm as a function of particle incidence angle  $\theta$  and  $\beta$ .

spectrometer. The detector performed well in the balloon-borne environment despite large variations in pressure and temperature. The RICH technique allows for the first time a reliable particle identification on an event-by-event basis necessary for identification of rare particles in a large background.

## References

- [1] J. Buckley et al., Nucl. Instr. and Meth. A 323 (1992) 380.
- [2] R.L. Golden et al., Nucl. Instr. and Meth. A 306 (1991) 366.
- [3] M. Hof et al., Nucl. Instr. and Meth. A 345 (1994) 561.
- [4] G. Barbiellini et al., Nucl. Instr. and Meth. A 333 (1993) 560.
- [5] G. Barbiellini et al., Nucl. Phys. C 32 (1993) 77.
- [6] D.F. Anderson, Phys. Lett. B 118 (1980) 230.
- [7] P. Carlson et al., Nucl. Instr. and Meth. A 349 (1994) 577.
- [8] H. Hempstead et al., Nucl. Instr. and Meth. A 306 (1991) 207.